Supplementary Material for Pressure sensitive ion-conduction in conical channel: optimal pressure and geometry

W.Q. Boon,[1, a)] T.E. Veenstra,[1, a)] M. Dijkstra,[2] and R. van Roij[1]
[1)] *Institute for Theoretical Physics, Utrecht University, Princetonplein 5, 3584 CC Utrecht, The Netherlands*
[2)] *Soft Condensed Matter, Debye Institute for Nanomaterials Science, Utrecht University, Princetonplein 1, 3584 CC Utrecht, The Netherlands*

(Dated: 24 August 2022)

I. POISSON-NERNST-PLANCK-STOKES EQUATION AND BOUNDARY CONDITIONS

In the main text we introduced an axially symmetric conical channel of length L, base radius R_b at $x=0$, and tip radius $R_\mathrm{t} \leq R_\mathrm{b}$ at $x=L$, with x the cartesian coordinate that runs along the symmetry axis. The channel connects two bulk reservoirs of an aqueous 1:1 electrolyte both at the same ionic bulk concentration $2\rho_b$. The viscosity is η, the ionic diffusion coefficient is D, the dielectric constant is ε, and the Debye length is $\lambda_D = \sqrt{\varepsilon k_B T/2\rho_b e^2}$ where T denotes room temperature, e the elementary charge, and k_B the Boltzmann constant. The channel has a fixed negative surface charge density $e\sigma$ at a radial distance $r=R(x)$ from the central axis, where $R(x) = R_\mathrm{b} - (x/L)(R_\mathrm{b}-R_\mathrm{t})$ for $x\in[0,L]$. We consider transport of solvent, ionic charge, and salt driven by the simultaneous application of a steady potential drop $\Delta\psi$ and a steady pressure drop ΔP. The transport is characterised by a volumetric flow rate Q, an electric current I, and a salt current J through the channel. Throughout we focus on the long-channel thin-EDL limit $\lambda_D \ll R_\mathrm{t} < R_\mathrm{b} \ll L$, and on the regime of low Reynolds number. We thus ignore overlap of the electric double layers (EDLs) and entrance effects.

In the steady state and the low Reynolds number of interest here, the force balance is given by the steady Stokes equation

$$\eta\nabla^2\mathbf{u} = \nabla P + e\rho_\mathrm{e}\nabla\psi, \tag{S1}$$

where $\mathbf{u}(x,r)$ is the fluid velocity, $P(x,r)$ the pressure, $\psi(x,r)$ the electrostatic potential, and $e\rho_\mathrm{e}(x,r)$ the ionic space charge density with $\rho_\mathrm{e} = \rho_+ - \rho_-$ and $\rho_\pm(x,r)$ the cationic (+) and anionic (-) concentration profile. The first term on the right hand side of Eq. (S1) will mainly be driven by a pressure drop and causes a Poiseuille-like flow through the channel, and the second term represents an electric body force that is mainly driven by a potential drop and causes an electro-osmotic flow as we will see below. In thermodynamic equilibrium, where $\mathbf{u}=\mathbf{0}$, the pressure gradient balances the electric body force.

The ionic fluxes $\mathbf{j}_\pm$ contain a Fickian diffusive, an Ohmic conductive, and Stokesian advective contribution described by the Nernst-Planck equations

$$\mathbf{j}_\pm = -D\left(\nabla\rho_\pm \pm \rho_\pm\frac{e\nabla\psi}{k_BT}\right) + \rho_\pm\mathbf{u}, \tag{S2}$$

where D is the diffusion coefficient that is assumed to be equal for both ionic species for convenience. In the electrolyte the electric potential satisfies the Poisson equation

$$\nabla^2\psi = -\frac{e}{\varepsilon}\rho_\mathrm{e}, \tag{S3}$$

and on the channel wall, at $r=R(x)$ with $x\in[0,L]$ and surface normal $\mathbf{n}$ pointing into the channel, we impose Gauss law $\mathbf{n}\cdot\nabla\psi = e\sigma/\varepsilon$. Note that this form of Gauss law implicitly assumes that the dielectric constant of the electrolyte is much larger than that of the wall material, such that the electric field lines do not "leak" out of the channel. The electrolyte is treated as incompressible, and together with the steady-state of interest this yields the divergence-free flux conditions

$$\nabla\cdot\mathbf{u} = 0; \quad \nabla\cdot\mathbf{j}_\pm = 0. \tag{S4}$$

On the channel walls we also impose no-slip boundary and blocking conditions $\mathbf{u}=0$ and $\mathbf{n}\cdot\mathbf{j}_\pm = 0$. Deep into the bulk of the reservoir connected to the base, $x \ll -L$, we impose $\rho_\pm = \rho_\mathrm{b}$, $\psi = \Delta\psi$, $P = P_0 + \Delta P$ with P_0 an arbitrary reference pressure, and deep into the reservoir connected with the tip, $x \gg L$, we impose $\rho_\pm = \rho_\mathrm{b}$, $\psi = 0$, and $P = P_0$.

The analysis of the PNPS equations is greatly facilitated by the linear combinations given by the total local salt concentration $\rho_\mathrm{s} = \rho_+ + \rho_-$, the ionic charge flux density $\mathbf{j}_\mathrm{e} = \mathbf{j}_+ - \mathbf{j}_-$, and the salt flux density $\mathbf{j}_\mathrm{s} = \mathbf{j}_+ + \mathbf{j}_-$, in terms of which the Nernst-Planck equations (S2) can be rewritten as

$$\mathbf{j}_\mathrm{e} = -D\big(\nabla\rho_\mathrm{e} + \rho_\mathrm{s}\frac{e\nabla\psi}{k_\mathrm{B}T}\big) + \mathbf{u}\rho_\mathrm{e}, \tag{S5}$$

$$\mathbf{j}_\mathrm{s} = -D\big(\nabla\rho_\mathrm{s} + \rho_\mathrm{e}\frac{e\nabla\psi}{k_\mathrm{B}T}\big) + \mathbf{u}\rho_\mathrm{s}. \tag{S6}$$

Here we note that the conduction terms $\propto\nabla\psi$ are proportional to ρ_s for the electric flux and to ρ_e for the salt flux. This coupling will prove to be key to understanding the physics of the cone-shaped channel. In the main manuscript, we refer to Eqs. (S1)-(S6) and their boundary conditions as the Poisson-Nernst-Planck-Stokes (PNPS) equations.

II. DERIVATION ELEMENTS ONSAGER MATRIX

Here we will discuss the details and assumptions involved in the derivation of Eqs. (1)-(3) of the main text and the components $\mathbb{L}_{11}, \mathbb{L}_{12}$ and $\mathbb{L}_{22}$ of the Onsager-like matrix starting from the PNPS equations (S1)-(S6). The

[a)] These two authors contributed equally

hierarchy of length scales $L \gg R_b \geq R_t > \lambda_D$ serves as the starting point of our derivation. When the channel is much longer than the largest radius $L \gg R_b$ entrance-outlet effects to the conductance can be neglected. Additionally, in the long-channel limit all radial components of fluxes and gradients are expected to be much smaller than the corresponding lateral components. Combined with the thin-EDL limit $\lambda_D \ll R_t$, which is motivated by the experimental conditions in Ref.[1], this ensures that the local ion concentrations and the electric field are essentially equal to the cross-sectional averaged salt concentration and electric field, so $\rho_s(x,r) \simeq \bar{\rho}_s(x) = 2\pi \int_0^{R(x)} \rho_s(x,r) r dr / \pi R^2(x)$ and $\partial_x \psi(x,r) \simeq \partial_x \bar{\psi}(x) = 2\pi \int_0^{R(x)} \partial_x \psi(x,r) r dr / \pi R^2(x)$. Moreover, the thin-EDL limit does not only allow us to neglect the influence of channel curvature on the EDL, but also allows us to neglect the influence of salt adsorption[2] on the cross-sectional averaged salt concentration $\bar{\rho}_s(x)$. Hence by using the thin-EDL assumption we neglect the inhomogeneous advection of salt through the EDL. For

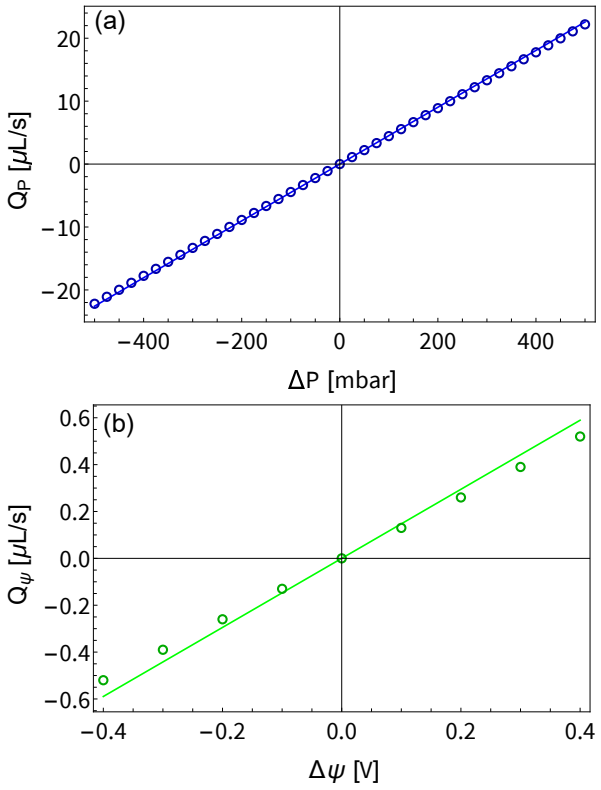

FIG. S1. (a) Poiseuille-like fluid flux Q_P as a function of the pressure drop ΔP at vanishing potential drop $\Delta\psi = 0$ and (b) electro-osmotic potential driven fluid flux Q_ψ as a function of the potential drop $\Delta\psi$ at a vanishing pressure drop $\Delta P = 0$, both for our standard parameter set (see Letter) and obtained from numerical solution of the full PNPS equations (S1)-(S6) (symbols) and from $\mathbb{L}_{11}$ and $\mathbb{L}_{12}$ (lines), respectively. Both fluid fluxes are linear in their respective driving force. There is good agreement between analytic and numerical results for the pressure driven flow Q_P, however the analytic expression for the electro-osmotic flow Q_ψ overestimates the flow rate by $\sim 10\%$.

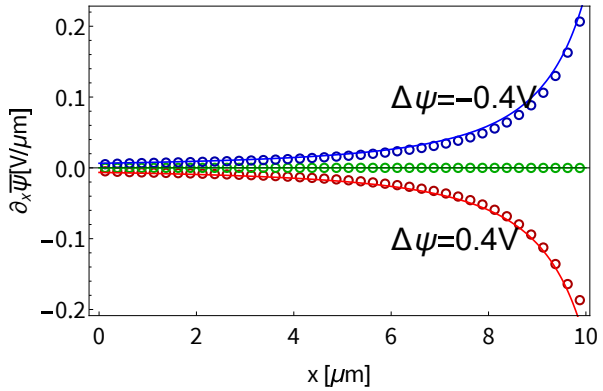

FIG. S2. The electric field $-\partial_x\bar{\psi}(x)$ for our standard parameter set with pressure drop $\Delta P = 0$ as a function of the lateral position x for $\Delta\psi = \pm 0.4$V and 0 volt (green) obtained from full numeric solutions of the PNPS equations(S1)-(S6) (symbols) and Eq. (2) (line) for our standard parameter set (see Letter). Good agreement between numeric and analytic results is found, which confirms the accuracy of Eq. (2)

.

Debye lengths orders of magnitude smaller than the pore radius we expect this assumption to be quite robust, however it will break down at extremely high surface potentials $e\psi_0/k_BT \gg 1$ as in this regime salt adsorption grows exponentially with ψ_0. In summary using the approximations $\rho_s(x,r) \simeq \bar{\rho}_s(x)$, $\partial_x\psi(x,r) \simeq \partial_x\bar{\psi}(x)$, $\lambda_D \ll R_t$ in conjunction with the observation from numerical calculations that $|\rho_e(r \ll R(x))| \ll |\sigma/R(x)|$ will readily result in Eq. (3) upon radially integrating Eq. (S6).

Before calculating the fluid flux Q, we have to verify that the linear response relation Eq. (1) in the main text is valid for flow, as in the literature there is experimental and numerical evidence that electro-osmotic flow can invert in conical pores under certain experimental conditions[3–5]. This would have a dramatic impact on the pressure sensitivity of the cone. However, as can be seen in Fig. S1 we find that in the experimental regime of Ref. [5] no flow inversions occur as Q is linear in both the pressure and potential drop. It should be noted that any non-linearity in the fluid flow $Q(\Delta P, \Delta\psi)$ will significantly change the current-pressure relation $I(\Delta P, \Delta\psi)$.

Having verified that the flow Q is linear in their respective driving forces, it now remains to find expressions for first $\mathbb{L}_{11}$ and then $\mathbb{L}_{12}$. When the channel has a tip radius of zero and vanishing surface charge an expression for the fluid flux $Q_P = (\pi R_t R_b/L)\mathbb{L}_{11}\Delta P$ is known[6–8]. Modifying this solution by replacing the pore length L' of a channel with a tip radius of zero with our actual channel length $L = L'(R_b - R_t)/R_b$ (with $L' \geq L$) representative of a channel with the same opening angle $2\alpha = 2\tan^{-1}(R_b/L') = 2\tan^{-1}((R_b - R_t)/L)$ but now a non-zero tip radius, we find

$$Q_P(\Delta P) = \frac{\Delta P}{\eta} \frac{3\pi L^3 R_b^3 R_t^3 \alpha^4}{8(R_b - R_t)^4 (R_b^2 + R_b R_t + R_t^2)}, \qquad \text{(S7)}$$

which for $R_b - R_t \ll L$ reduces to $\mathbb{L}_{11}$ in the main text. The agreement between this expression for the pressure-driven fluid flux Q_P (solid line) and the numerically obtained flow (symbols) is remarkable and can be seen in Fig. S1(a).

We now continue with the calculation of the electro-osmotic flow Q_ψ which first requires an expression for the electric field $-\partial_x\bar{\psi}(x)$ given in the main text by Eq. (2). This equation is valid under two conditions, (i) no electric field lines permeate the channel wall, and (ii) the space charge outside of the EDL is negligible. The first condition ensures that all electric field lines remain in the channel and holds when the dielectric constant of the channel wall is much smaller than that of the solvent. The second condition ensures that the divergence of the electric field is zero $\nabla\cdot\nabla\psi(x,r)=0$, for all r several Debye length away from the channel wall, ensuring that no new field lines appear. For straight channels this is a natural assumption, however in conical channels the lateral variation of the electric current $I(x)$ could allow for the build-up of space charge in principle. In our discussion of the numerical results we verify that the effect of this space charge is small and can largely be ignored in the parameter regime of our prime interest. When both condition (i) and (ii) are met the number of electric field lines remains constant over the channel length and the total lateral electric field through a radial slice multiplied by the area of the slice likewise has to be constant, $\pi R^2(x)\partial_x\bar{\psi}(x) = \text{constant}$. Now the electric field as function of lateral position can be found by observing that over the length of the pore the total potential drop has to equal to $\Delta\psi = -\int_0^L \partial_x\bar{\psi}\mathrm{d}x$, resulting in Eq. (2) of the Letter. In Fig. S2 we compare $\partial_x\bar{\psi}$ of Eq. (2) (solid lines), with the numerically obtained function $\partial_x\psi(x,r=0)$ along the symmetry axis in calculations for $\Delta P = 0$ (symbols) and find excellent agreement.

In order to calculate $\mathbb{L}_{12}$ from the electric field we use the solution for the potential-driven flow through a cylindrical pore but now with position dependent radius and electric field $-\partial_x\bar{\psi}(x)\pi R^2(x)(\varepsilon\psi_0/\eta)^2$ and observe that it is constant over the length of the pore as $\partial_x\bar{\psi}\propto 1/(\pi R^2(x))$. Hence this Ansatz yields a bonafide divergence-free electro-osmotic flow given by

$$Q_\psi(\Delta\psi) = -\frac{\Delta\psi}{L}\pi R_t R_b\frac{\varepsilon\psi_0}{\eta}, \tag{S8}$$

where we neglected terms of order λ_D/R on the basis of the thin-EDL limit. In Fig. S1(b) it can be seen that there is a minor deviation of $\sim 10\%$ between Q_ψ obtained from numerical calculations and this analytic approximation. Implicitly the PNPS equations (S1)-(S6) allow for diffusio-osmotic fluid flow, driven by the concentration gradient $\partial_x\bar{\rho}_s$. As the concentration profile and hence the gradient is a non-linear function of the potential drop, any diffusio-osmotic flow would manifest as a non-linear contribution to $Q_\psi(\Delta\psi)$. As no significant deviation from linearity is observed in our numerical results for $Q_\psi(\Delta\psi)$ we neglect diffusio-osmotic flow.

Having found expressions for both $\partial_x\bar{\psi}$ and Q we can now straightforwardly solve Eq. (3), directly yielding Eq. (4) of the main text. We compare Eq. (4 (solid lines) with the concentration from numerical calculations in Fig. S3 (symbols) for several ΔP and $\Delta\psi$. We see that while the agreement is not perfect both the non-monotonic ΔP trend and the overall shape of the concentration profile are captured rather reasonably. It can also be seen that the boundary condition used for analytic calculations ($\rho_s(0)=\rho_s(L)=2\rho_b$) are not fully representative of the numerical calculations, as the concentration profile extends a small distance out of the channel. This discrepancy is possible as in the numerical calculations we apply the boundary condition of bulk concentrations far away rather than at the channel edges. The description of the concentration profiles extending out of the in- and outlets of the conical pore would require a full description of the flow, electric field and currents at the edges of the cone which is not tractable analytically. More significant than the deviation at the tip and base is the sign change of the bulk-excess concentration profile when going from positive ΔP to $\Delta P \ll -50$mbar, a feature our analytic theory cannot explain. The deviation occurs at very large negative Péclet number and represents a secondary non-linearity unrelated to the non-linearity reported in the main text. We speculate the non-linearity may be due to the inhomogeneous advection current $\partial_x I_{adv} \propto \partial_x(2Q\sigma/R) \neq 0$ that can build up signif-

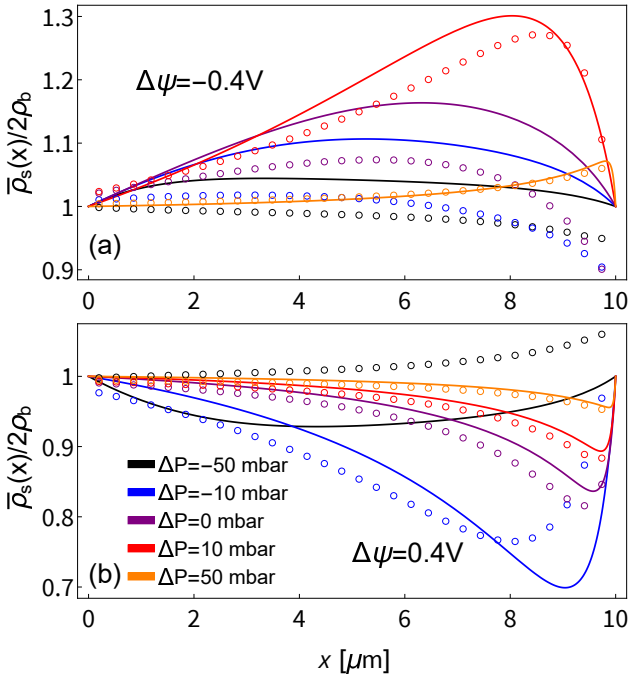

FIG. S3. Cross-sectional averaged concentration profile $\bar{\rho}_s(x)$ over the full channel length from numerical calculations of the full PNPS equations (symbols) compared to curves plotted with Eq. (4) for our standard parameter set (see main text), potential drop $\Delta\psi=-0.4$V (a) and $\Delta\psi=0.4$V (b) and varying pressure drop ΔP. Numeric and analytic results agree for positive ΔP but deviate for increasing negative ΔP. Concentration profiles are largest for $\Delta P = \mp 10$ mbar which is rather close to $\Delta P^* = \mp 13$ mbar, where fluid flow vanishes.

icant space-charge $\rho_e(x,r)$ outside the EDL. To study this secondary non-linearity in full detail would require solving for $\partial_x I = 0$ and $\partial_x J = 0$ simultaneously. While striking, the opposite sign of our deviation from bulk concentration in our analytic and numeric concentration around Pe$\ll -1$ has little influence on the current I, as the concentration deviation is an order of magnitude smaller than the concentration change around Pe = 0. In summary we identify three major sources of error (i) our analytic expression underestimates electro-osmotic flow Q_ψ by about 10% (ii) imposing bulk concentrations on the channel edges $\bar{\rho}_s(0) = \bar{\rho}_s(L) = 2\rho_b$ implicitly neglects edge effects, and (iii) neglecting minor secondary non-linearities, which are probably related to the lateral variation of the current $I(x)$ that are to be compensated by a (small) space charge distribution $\bar{\rho}_e(x)$. A final limitation of our theory is that for large negative $\Delta\rho$ the theory allows for $\bar{\rho}_s(x)$ to become locally negative, which is clearly unphysical. This unphysical result can emerge because the Debye length increases when the concentration decreases, eventually invalidating our starting assumption $\lambda_D \ll R$. Care should thus be taken not to use the theory in this regime, with a negative conductance a hallmark that the range of validity has been exceeded. Throughout we restrict attention to concentration profiles that deviate less than about 30% from the bulk concentration, which also allows for equating the relative change of the channel conductance to (the negative of) the change of the relative channel resistance.

To calculate the last matrix element $\mathbb{L}_{22}$ we radially integrate Eq. (S5), resulting in a diffusive, conductive and advective current. In our discussion of numerical results we show that the diffusive current is negligible, which is consistent with the assumption of a negligible space charge outside the EDL, $\rho_e(r \ll R - \lambda_D, x) \approx 0$. This leaves two components of the current to be calculated $I = I_{cond} + I_{adv}$ whose ratio scale as $I_{adv}/I_{cond} \propto \lambda_D/R$ allowing us to neglect the advective component to $\mathbb{L}_{22}$ when $\lambda_D/R \ll 1$. Now the total current due to a potential drop $\Delta\psi$ is straightforwardly found by integration of the conductive component $-(De/k_BT)\rho_s(x,r)\partial_x\psi(x,r)$ in Eq. (S6) and by using $\rho_s(r,x) \simeq \bar{\rho}_s(x)$ and $\psi(r,x) \simeq \bar{\psi}(x)$ we find

$$I_{cond}(x) = eD\frac{e\Delta\psi}{k_BT}\frac{\pi R_t R_b}{L}\bar{\rho}_s(x), \tag{S9}$$

which is inhomogeneous for any non-constant $\bar{\rho}_s(x)$. This inhomogeneity will lead to formation of a space charge ρ_e outside the EDL. However, in our discussion of numerical results we will show that this space charge is small. By treating the concentration profile as a collection of resistors in series[2] we can obtain the ultimate, laterally constant current. From this it follows that $\bar{\rho}_s(x)$ in Eq. (S9) should be replaced by the inverse average $L/\int_0^L(\bar{\rho}_s(x)^{-1}\mathrm{d}x$ which is close to the lateral average $\langle\bar{\rho}_s\rangle$ as long as $|\log(\bar{\rho}_s(x)/(2\rho_b)| < 1$. The error of this approximation diverges when $\bar{\rho}_s(x)/2\rho_b$ approaches zero. As in the Letter we restrict attention to concentration profiles that deviate less than about 30% from the bulk concentration a regime for which this approximation is very reasonable.

Having already calculated $\mathbb{L}_{12}$ for the electro-osmotic flow Q_ψ we can invoke Onsager's reciprocal relation, which states that $\mathbb{L}_{21} = \mathbb{L}_{12}$[9,10], to find the fully advective pressure-driven current and obtaining the full current

$$I(\Delta\psi,\Delta P) = \frac{\pi R_t R_b}{L}\left(\frac{e^2 D\Delta\psi}{k_BT}\langle\bar{\rho}_s\rangle - \Delta P\frac{\varepsilon\psi_0}{\eta}\right). \tag{S11}$$

Finally, combining $\mathbb{L}_{11}$, $\mathbb{L}_{12}$ and $\mathbb{L}_{22}$ our ultimate expression for the Onsager-like matrix Eq. (1) reads

$$\frac{\pi R_b R_t}{L}\begin{pmatrix}\frac{R_b^2 R_t^2}{8\eta\langle R^2\rangle} & -\frac{\varepsilon\psi_0}{\eta}\\ -\frac{\varepsilon\psi_0}{\eta} & \frac{e^2 D}{k_BT}\langle\bar{\rho}_s\rangle\end{pmatrix}\begin{pmatrix}\Delta P\\ \Delta\psi\end{pmatrix} = \begin{pmatrix}Q\\ I\end{pmatrix}. \tag{S12}$$

III. IDEAL PORE GEOMETRY

As the deviation of Ohmic current is largest when the difference between the laterally-averaged concentration $\langle\bar{\rho}_s\rangle$ and bulk concentration $2\rho_b$ is largest it is interesting to note that an analytic expression for $\langle\Delta\bar{\rho}_s\rangle = \langle\bar{\rho}_s\rangle - 2\rho_b$ is available in the limit Pe = 0, which is the limit near which the concentration difference is largest,

$$\langle\Delta\bar{\rho}_s\rangle = \frac{e\Delta\psi}{k_BT}\frac{\sigma}{R_t}\frac{\frac{R_t}{R_b}\left(2(\frac{R_t}{R_b}-1) - \left(1+\frac{R_t}{R_b}\right)\log\left(\frac{R_t}{R_b}\right)\right)}{(1-\frac{R_t}{R_b})^2}. \tag{S13}$$

The prefactor $(e\Delta\psi/k_BT)(\sigma/R_t)$ is the tip Duhkin number times the dimensionless potential drop and bulk concentration, which diverges for vanishing tip radius, indicating that for the maximum non Ohmic conductivity the tip size should be as small as possible. However as we assumed a thin-EDL limit from the very beginning this prediction only remains valid as long as $R_t \gg \lambda_D$. We estimate that optimization of non-linear current by minimization of the tip radius holds up to $R_t \approx 10\lambda_D$. It is easily checked that for fixed tip radius $\langle\Delta\bar{\rho}_s\rangle$ of Eq. (S13) has a maximum at $R_t/R_b \simeq 0.22$, a geometry which hence optimizes diodic behavior. Furthermore, while $\Delta\rho$ as defined by Eq. (5) in the main text is a measure for the concentration profile the ratio $\Delta\rho/\langle\bar{\rho}_s\rangle$ is large, with the proportionality constant between the two at zero flow being given by

$$\frac{\Delta\rho}{\langle\Delta\bar{\rho}_s\rangle} = \frac{2(R_t/R_b)^{-2}(1-\frac{R_t}{R_b})^3}{2\frac{R_t}{R_b} - 2 - (1+\frac{R_t}{R_b})\log(\frac{R_t}{R_b})}, \tag{S14}$$

which for straight pores with $R_t \simeq R_b$ equals 12 and in the limit $R_t/R_b \ll 1$ is well approximated by $\Delta\rho/\langle\Delta\bar{\rho}_s\rangle \simeq 2R_b^2/R_t^2\log(R_b/R_t)$ which diverges for large base

radii. Hence for conical pores in general $\Delta\rho \gg 12\langle\bar{\rho}_s\rangle$ and for our standard parameter set in the main text $\Delta\rho/\langle\Delta\bar{\rho}_s\rangle \simeq 100.9$ while for the optimal tip-to-base ratio $\Delta\rho/\langle\Delta\bar{\rho}_s\rangle \simeq 68.3$. In principle one could absorb the proportionality constant Eq. (S14) in the definition of $\Delta\rho$ to obtain a measure that accurately represents the laterally-averaged concentration profile $\langle\Delta\bar{\rho}_s\rangle$.

At finite Pe no analytic expression for $\langle\Delta\bar{\rho}_s\rangle$ can be found, but its value can be straightforwardly calculated by numerical integration. In Fig. S4(a) we plot $[(k_B T R_t)/(e\Delta\psi\sigma)]\langle\Delta\bar{\rho}_s\rangle$ against R_t/R_b for Pe $\in [0, 10^3]$. At Pe = 0 (blue line) the maximum laterally averaged concentration is found at a tip-to-base ratio $R_t/R_b \simeq 0.22$ (vertical line). As observed in Eq. (S13) for non-zero Péclet number the ideal tip-to-base ratio (symbols) is always smaller than 0.22. Note that when no pressure drop ΔP^* is applied the Péclet number will scale with $\Delta\psi$ and the ideal pore geometry thus depends on the voltage operating range of a device. In Fig. S4(b) we plot the optimal tip-to-base ratio R_t/R_b against Péclet number on a linear-logarithmic scale. It can be seen that for small |Pe|$\leq$ 10 the ideal ratio 0.22 holds, but for large Pe it decays algebraically to zero. In Fig. S4(c) we plot the same data as in (b) but now in a log-log representation to highlight the scaling in the Pe $\geq$ 100 regime. We find that the relation between optimal geometry and Pe is well described by a power law $b|\mathrm{Pe}|^{-\nu}$ in this regime, with $b \simeq 2.5$, $\nu \simeq 0.9$ for positive and $b \simeq 0.9$, $\nu \simeq 0.55$ for negative Péclet.

IV. DISCUSSION NUMERICAL RESULTS

Here we will discuss the numerical results of the full PNPS equations (S1)-(S6) in depth and show that the effect of the space charge outside the EDL on the current I can be neglected. In Fig. S5 we plot our numerical solutions of the pressure excess electric current $I_P = I(\Delta P, \Delta\psi) - I(0, \Delta\psi)$ as a function of the pressure drop ΔP for our standard parameter set and (a) $\Delta\psi = 0$, (b) $\Delta\psi = +0.4$V, and (c) $\Delta\psi = -0.4$V. When no potential drop is applied we find that the electric current is linear in the pressure drop and dominated by advection, as can be seen in Fig. S5(a) where we plot $I_P(\Delta P, \Delta\psi)$, split into its diffusive, conductive and advective components. When the pressure drop is applied in conjunction with a potential drop we find that it is strongly non-linear, as can be seen Fig. S5(b) and (c). A minimum in the total current is found at $\Delta P = \mp 10$ mbar for $\Delta\psi = \pm 0.4$V in Fig. S5(b) and (c), and near the minimum the conductive current dominates over the advective and diffusive currents. For pressure drops larger than $|\Delta P|$>100 mbar the advective current I_P dominates and follows the linear relation observed for $\Delta\psi = 0$ shown in Fig. S5(a). The non-linearities in (b) and (c) are mainly due to the conductive component $-(De/k_B T)\rho_s(x,r)\partial_x\psi(x,r)$ of the electric current Eq. (S5) which depends not only on the salt concentration $\rho_s(x,r)$ but also the electric field $-\nabla\psi(x,r)$. Inspecting Fig. S6, where we plot the ΔP-dependence of the current, the salt concentration, and the electric field at $x = 0.9L$ all normalized by their values at vanishing pressure drop, we indeed find that both the salt concentration $\bar{\rho}_s$ as well as the electric field $-\partial_x\bar{\psi}$ vary with ΔP. However, we find that the variation of the electric field is ~ 5 times smaller than the change of concentration with pressure, and actually opposes the non-linearity of the conduction current for $\Delta\psi = -0.4$V.

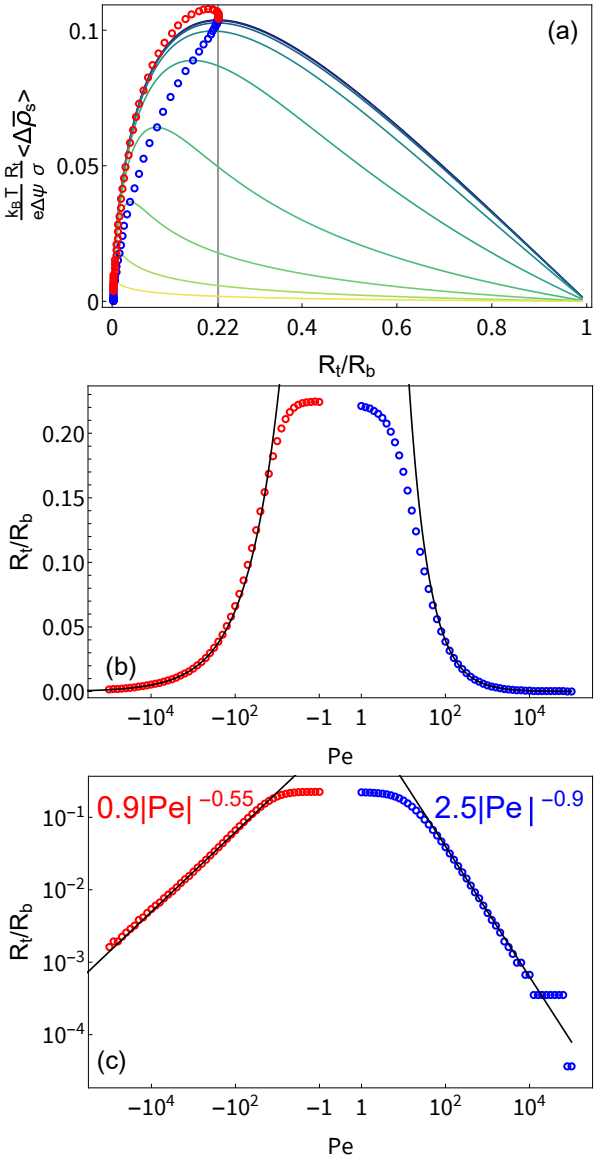

FIG. S4. (a) Laterally averaged concentration $\langle\bar{\rho}_s\rangle$ normalized by $(\sigma/R_t)(e\Delta\psi/k_B T)$ for varying tip-base ratio R_t/R_b with the Péclet number between curves varying by $10^{1/2}$ with the yellow curve corresponding to Pe= 10^3 and blue curve with Pe=10^{-1} closely matching Eq. (S13). Blue points denote optimal tip-to-base ratios for Pe$\in [10^{-1}, 10^5]$ and red points denote optima for Pe$\in [-10^{-1}, -10^5]$, with optimal ratios $R_t/R_b \ll 1$ corresponding to Pe$\gg 1$. (b) Optimal tip-to-base ratio for varying Péclet in log-linear representation, with red points at negative Pe and blue at positive Pe. Black lines represent power-laws whose scaling is found was found in (c) by fitting the data in log-log representation. For large positive Pe the optimal tip-to-base ratio scales as $R_t/R_b \simeq 2.5|\mathrm{Pe}|^{-0.9}$ while for large negative Pe it is well approximated by $R_t/R_b \simeq 0.9|\mathrm{Pe}|^{-0.55}$.

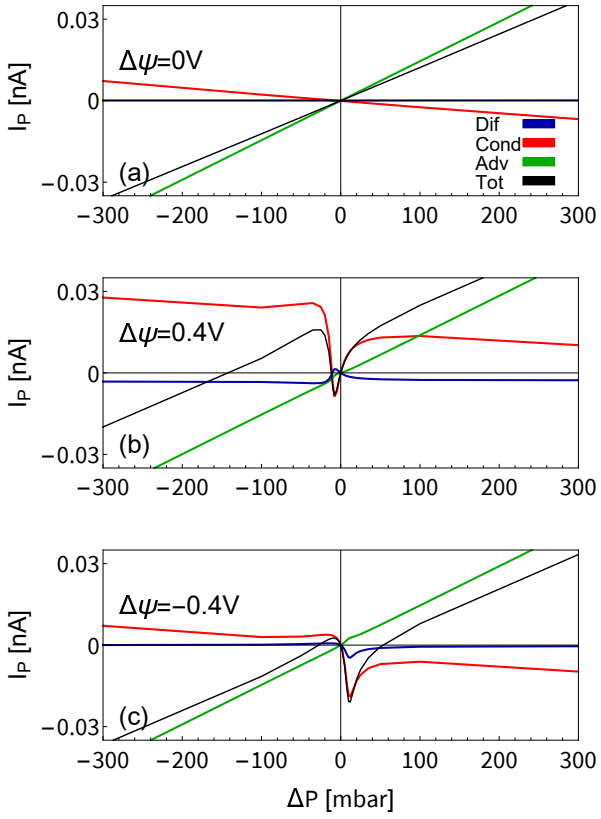

FIG. S5. Total pressure excess diffusive, conductive, advection and net electric current (respectively Dif, Cond, Adv and I_P) at $x = 0.9L$ from numerical solutions of the full PNPS equations (S1)-(S6) as function of the pressure drop ΔP offset by the current at $\Delta P = 0$ for our standard set of parameters in the main text. For (a) where $\Delta\psi = 0$ the current is linear in ΔP and dominated by the advective current. For (b) and (c), where respectively $\Delta\psi = +0.4$V and $\Delta\psi = -0.4$V, the current is non-linear for low pressure drops ($|\Delta P|$<50 mbar) and here conductive current dominates the non-linear pressure-current relation, with diffusive and advective components only marginally contributing. At large pressures the net current is again dominated by the advective, streaming current, current which follows the same linear trend found for $\Delta\psi = 0$.

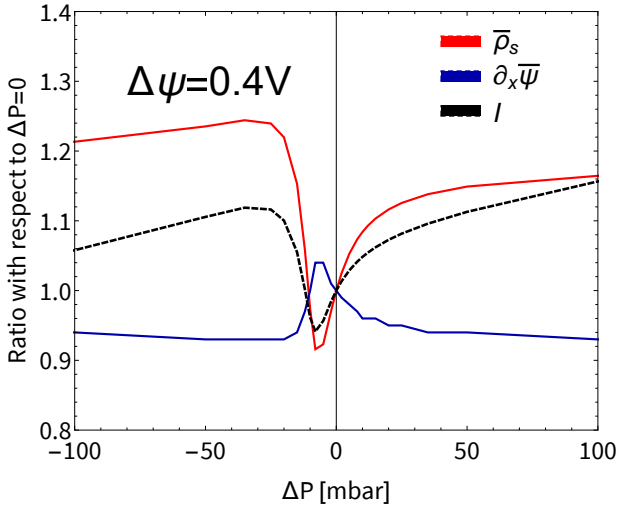

FIG. S6. Pressure drop dependence of the cross-sectional averaged electric field $\partial_x\bar{\psi}$, salt concentration $\bar{\rho}_s$, and total current I, all normalized with their respective values at $\Delta P = 0$, at lateral position $x = 0.9L$ and for a potential $\Delta\psi = 0.4$V, as obtained from numerical solutions of the full PNPS equations (S1)-(S6) for our standard parameter set (see main text). The relative deviations from unity are much larger for the salt concentration and the current than for the electric field; in fact the current correlates well with the salt concentration and even anti-correlates with the electric field.

As the change in electric field actually counter-acts the non-linearity observed in the electric current we conclude that the ΔP dependency of $\partial_x\bar{\psi}$ cannot be the dominant driving force behind the non-linear current $I(\Delta P)$. This suggests that the non-linear current I can be essentially understood by considering the dependency of the salt density ρ_s on $\Delta\psi$ and ΔP, with the space charge density ρ_e outside of the EDL only contributing minutely to the non-linearity both through diffusive I_{dif} and advective I_{adv} currents as well as pressure dependent electric field $-\partial_x\bar{\psi}$. Hence Fig. S6 shows that dependency of space charge ρ_e on ΔP only leads to negligible variation in the magnitude of diffusive and advective current I_{dif} and I_{adv} as seen in Fig. S5(b) and (c). The conclusion that space charge is negligible is based on an empirical observation of numerical results, so we cannot rule out that there are regimes in which space charge does dominate the non-linear current. However, as we have chosen a set of parameters to reproduce the experimental set-up of Ref.[1] we can conclude that for this specific set of experiments space charge is negligible and not of key importance to the non-linear current $I(\Delta P)$. We conclude from these numerical results that (i) the conductive component of the electric current is responsible for the extremely mechanosensitive current observed in experiments, (ii) changes in the electric field and space-charge density with pressure are small and can be neglected, and (iii) the pressure-sensitivity of the electric-field and space charge actually (weakly) oppose the non-linear conduction current and thus cannot be responsible for the observed non-linear current.

[1] L. Jubin, A. Poggioli, A. Siria, and L. Bocquet, Proceedings of the National Academy of Sciences **115**, 4063 (2018).
[2] B. L. Werkhoven and R. van Roij, Soft Matter **16**, 1527 (2020).
[3] N. Laohakunakorn, V. V. Thacker, M. Muthukumar, and U. F. Keyser, Nano Letters **15**, 695 (2015).
[4] W.-J. Lan, M. A. Edwards, L. Luo, R. T. Perera, X. Wu, C. R. Martin, and H. S. White, Accounts of Chemical Research **49**, 2605 (2016).
[5] G. W. Bishop, M. M. Lopez Jr, P. Ramiah Rajasekaran, X. Wu, and C. R. Martin, The Journal of Physical Chemistry C **119**, 16633 (2015).
[6] M.-S. Chun, S.-Y. Lee, and S.-M. Yang, Journal of Colloid and Interface Science **266**, 120 (2003).
[7] J. Happel and H. Brenner, *Low Reynolds number hydrodynamics: with special applications to particulate media*, Vol. 1 (Springer Science & Business Media, 2012).
[8] T. E. Veenstra, *Strongly Non-Linear Pressure-Induced Ion Currents in Conical Nanopores*, BSc thesis (2020).
[9] H. B. G. Casimir, Reviews of Modern Physics **17**, 343 (1945).
[10] L. Onsager and S. Machlup, Physical Review **91**, 1505 (1953).